

Article

Charactering the metabolism of cryptotanshinone by human P450 enzymes and uridine diphosphate glucuronosyltransferases *in vitro*

Jin ZENG[#], Yu-juan FAN[#], Bo TAN, Hui-zong SU, Yue LI, Lin-lin ZHANG, Jian JIANG^{*}, Fu-rong QIU^{*}

Department of Clinical Pharmacology, Shuguang Hospital, Shanghai University of Traditional Chinese Medicine, Shanghai 201203, China

Abstract

Cryptotanshinone (CT) is the main active component in the root of *Salvia miltiorrhiza* Bunge (SMB) that displays antibacterial, anti-inflammatory and anticancer activities. In this study, we characterized phase I and phase II metabolism of CT in human liver microsomes *in vitro* and identified the metabolic enzymes (CYPs and UGTs) involved. The metabolites of CT generated by CYPs were detected using LC-MS/MS and the CYP subtypes involved in the metabolic reactions were identified using chemical inhibitors of CYP enzymes and recombinant human CYP enzymes (CYP1A2, CYP2A6, CYP2C8, CYP2C9, CYP2C19, CYP2D6, and CYP3A4). Glucuronidation of CT was also examined, and the UGT subtypes involved in the metabolic reactions were identified using recombinant human UGT enzymes (1A1, 1A3, 1A4, 1A5, 1A6, 1A7, 1A8, 1A9, 1A10, 2B4, 2B7, 2B15 and 2B17). After adding NADPH to the human liver microsomes incubation system, CT was transformed into 6 main dehydrogenation and hydroxylation metabolites. CYP2A6, CYP3A4 and CYP2C19 were the major contributors to the transformation of its hydroxylation metabolites. CYP2C19, CYP1A2 and CYP3A4 were the major contributors to the transformation of its hydrogenation metabolites in human liver microsomes. This study showed that the metabolites at *m/z* of 473 were mediated by UGT1A9 and that the metabolites at *m/z* of 489 were mediated by UGT2B7 and UGT2B4. CT was extensively metabolized by UGTs following metabolism by CYPs in the liver.

Keywords: cryptotanshinone; P450 enzymes; uridine diphosphate glucuronosyltransferases; metabolic characteristics; human liver microsomes

Acta Pharmacologica Sinica (2018) 39: 1393–1404; doi: 10.1038/aps.2017.144; published online 8 Feb 2018

Introduction

The root of *Salvia miltiorrhiza* Bunge (SMB), a well-known traditional Chinese herbal medicine, has been widely used in China to treat coronary heart disease, cerebrovascular disease, hepatitis, hepatocirrhosis and chronic renal failure^[1]. Cryptotanshinone (CT) is the main active component of SMB and has attracted worldwide attention due to its pharmacological activities, including antibacterial^[2], anti-inflammatory^[3] and anticancer activities^[4,5].

Recently, the pharmacokinetic characteristics of cryptotanshinone have been studied in animals. The oral bioavailability of cryptotanshinone in pigs was extremely poor because the plasma concentration was almost undetectable at a dose of 40 mg/kg^[6]. Using HPLC-MS, the maximum plasma concentra-

tion (C_{max}) of cryptotanshinone was below 20 ng/mL after oral administration of total tanshinones (containing 12% of cryptotanshinone) to rats at a dose of 350 mg/kg^[7]. Our recent studies showed that the C_{max} of cryptotanshinone was below 20 ng/mL after oral administration of tanshinone capsules to healthy Chinese volunteers at a dose of 1000 mg (containing 88 mg cryptotanshinone)^[8]. Although the poor oral availability of cryptotanshinone has been partly explained by P-glycoprotein (P-gp)-mediated efflux^[9,10], cryptotanshinone might undergo extensive first-pass metabolism^[11]. Song *et al* reported six phase I metabolites of cryptotanshinone in pigs^[12]. Dai *et al* identified nineteen phase I and six phase II metabolites of cryptotanshinone in both *in vivo* and *in vitro* experiments in rats^[13]. Dehydrogenated and hydroxylated metabolites were the main phase I metabolites. Liu *et al* studied phase I and phase II metabolism both *in vitro* and *in vivo* for individual and mixed tanshinones in rats and found that oxidation and O-glucuronidation were the major pathways in phase I and phase II metabolism^[14]. However, no information is available regarding

[#]These authors contributed equally to this work.

^{*}To whom correspondence should be addressed.

E-mail: Jiangjiansg@126.com (Jian JIANG);

Furong_qiu@126.com (Fu-rong QIU)

Received 2017-06-20 Accepted 2017-10-26

the specific metabolites or which isozyme of cytochrome P450 (CYP) enzymes is involved in this reaction in humans.

Drug metabolism is classified into phase I and phase II metabolism. CYPs are the primary phase I enzymes that catalyze oxidation and reduction reactions. The CYP enzymes that contribute to phase I metabolism of drugs are often from the CYP1, 2 and 3 families and include CYP1A2, 2A6, 2C8, 2C9, 2C19, 2D6 and 3A4^[15]. Phase II metabolism (conjugation) often occurs in metabolites produced by phase I oxidation and in parent drugs bearing appropriate functional moieties, such as hydroxyl and carboxylic acid groups. UDP-glucuronosyl-transferase (UGT)-mediated glucuronidation is responsible for the clearance of 35% of drugs^[16]. In humans, enzymes from the UGT1A and 2B families are the main contributors to this type of drug metabolism. The CYP and UGT enzymes have been reported to contribute to the metabolism of over 80% of clinical drugs^[17]. Therefore, characterizing the metabolism of drugs by both CYPs and UGTs in humans is of great value.

As we know, tanshinone IIA is a dehydrogenated metabolite of cryptotanshinone, and this metabolite has many pharmacological activities^[18, 19], although the other main metabolites of cryptotanshinone might also have unreported pharmacological activities. Additionally, metabolite profiling is a useful tool for predicting the pharmacokinetic properties of drug candidates and assessing the possibility of drug-drug interactions (DDI). The purpose of this study was to characterize the cryptotanshinone metabolites in human liver microsomes (HLMs) and contribution to the metabolism of cryptotanshinone by CYPs and UGTs using HLMs and cDNA expressed enzymes.

Materials and methods

Chemicals

Cryptotanshinone, ketoconazole, and diazepam were purchased from National Institute for the Control of Pharmaceutical and Biological Products (Beijing, China). Furofylline, ticlopidine, sulfaphenazole, methoxsalen, quinidine, quercetin, dicumarol, chlorpromazine, diclofenac sodium, dimethyl sulfoxide (DMSO), NADPH, uridine diphosphoglucuronic acid (UDPGA), alamethicin and β -glucuronidase were purchased from Sigma-Aldrich (St Louis, MO, USA). Pooled HLMs ($n=10$), pooled human liver S9 fractions (S9) ($n=10$) and pooled cytosol ($n=10$) were purchased from the Rild Research Institute for Liver Diseases (Shanghai, China). HPLC-grade methanol and acetonitrile were purchased from Tedia Company (USA). Ammonium acetate and analytic grade formic acid were purchased from the China National Pharmaceutical Group Corporation. Deionized water was purified using a Milli-Q system (Millipore Corporation, France). cDNA-expressed human CYP enzymes (CYP3A4, CYP2A6, CYP2C8, CYP2C9, CYP2C19, CYP2D6, and CYP1A2) and cDNA-expressed human UGT enzymes (UGT1A1, 1A3, 1A4, 1A6, 1A7, 1A8, 1A9, 1A10, 2B4, 2B7, 2B15 and 2B17) were purchased from BD Biosciences (Woburn, MA, USA).

Phase I metabolism assay

A typical incubation mixture contained 40 μ L of human liver

microsomes (1 mg/mL), 20 μ L of NADPH (10 mmol/L), and 120 μ L of potassium phosphate (pH 7.4). The incubation mixture was preincubated at 37°C for 5 min. The reaction was initiated by the addition of 20 μ L of cryptotanshinone (100 μ mol/L) and terminated by the addition of 200 μ L ice-cold acetonitrile at predetermined time points. Control incubations were performed without NADPH.

Glucuronidation assay

The incubation mixture contained 40 μ L of microsomes (1 mg/mL), 10 μ L of $MgCl_2$ (200 μ mol/L), 10 μ L of saccharolactone (4.4 mmol/L), 20 μ L of NADPH (10 mmol/L), and 20 μ L of UDPGA (10 mmol/L) in 85 μ L of PBS (pH 7.4). The mixture was pretreated with 5 μ L of alamethicin (1000 μ g/mL) on ice to create pores and enhance the access of UDPGA and substrate to the UGT enzyme active site.

The incubation mixture was preincubated at 37°C for 5 min. The reaction was initiated by the addition of 10 μ L of cryptotanshinone (200 μ mol/L) and terminated by the addition of 200 μ L of ice-cold acetonitrile. Control incubations were performed without UDPGA. To confirm the formation of O-glucuronide, hydrolysis of the metabolite was performed using β -glucuronidase.

In all experiments, cryptotanshinone was dissolved in DMSO to obtain a 10 mmol/L stock solution and serially diluted to the required concentrations with PBS. The percentage of organic solvent in the incubation system did not exceed 0.1%.

Chemical inhibition analysis in HLMs

The contributions of CYP and UGT enzymes to cryptotanshinone metabolism were evaluated using inhibition experiments. The following specific chemical inhibitors were used: furofylline for CYP1A2, sulfaphenazole for CYP2C9, methoxsalen for CYP2A6, quercetin for CYP2C8, ticlopidine for CYP2C19, quinidine for CYP2D6 and ketoconazole for CYP3A4. Given the lack of specific inhibitors for UGTs, diclofenac sodium was used as the inhibitor for all of the UGTs because diclofenac sodium inhibits UGT1A9, 2B4 and 2B7^[20, 21]. Cryptotanshinone (final concentration: 10 μ mol/L) was used as the substrate. The substrate and inhibitors were preincubated in the incubation mixture with HLMs at 37°C for 5 min. NADPH (for CYPs, NADPH+UDPGA for UGTs) was then added to each reaction, and the reaction mixture was incubated for another 30 min. The final concentrations of ketoconazole, furofylline, quinidine, methoxsalen, quercetin, sulfaphenazole, ticlopidine and diclofenac sodium were 1, 10, 10, 10, 10, 5, and 300 μ mol/L, respectively. Incubation without the addition of inhibitors was used as the control.

Assay with recombinant human CYP enzymes

Incubation of each recombinant human CYP isoform was carried out as described in the microsomal study. Cryptotanshinone (10 μ mol/L) was incubated with each of the recombinant CYP enzymes (0.2 mg/mL) at 37°C for 30 min. Cryptotanshinone and its metabolites were measured in reaction mixtures

containing recombinant human CYP1A2, CYP2A6, CYP2C8, CYP2C9, CYP2C19, CYP2D6 and CYP3A4.

Glucuronidation assay with recombinant UGTs

First, 40 μL of human liver microsomes (1 mg/mL), 10 μL of cryptotanshinone (200 $\mu\text{mol/L}$) and 130 μL of potassium phosphate (pH 7.4) were added to a 1.5 mL Eppendorf tube that had been preincubated at 37°C for 5 min. The reaction was initiated by the addition of 20 μL of NADPH (10 mmol/L), preincubated at 37°C for 5 min, incubated in the mixture with HLMs at 37°C for 40 min and terminated by adding 200 μL of ice-cold acetonitrile at predetermined time points. The solution sample was freeze dried to dryness, the dried residue was dissolved in 100 μL of PBS and 20 μL of human liver cytosol was added as the NQO1 donor^[22]

A panel of commercially available UGT isoforms, including UGT1A1, UGT1A3, UGT1A4, UGT1A6, UGT1A7, UGT1A8, UGT1A9, UGT1A10, UGT2B4, UGT2B7, UGT2B15, and UGT2B17 (40 μL , 0.2 mg/mL), was screened for cryptotanshinone glucuronidation. The reaction was initiated by incubation at 37°C in 20 μL of NADPH and 20 μL of UDPGA (10 mmol/L) and terminated by adding 200 μL of ice-cold acetonitrile containing the internal standard diazepam at predetermined time points (0 min and 40 min).

Chemical inhibition analysis in S9

Selective chemical inhibitors were used to investigate the enzymes responsible for reduction of cryptotanshinone and its phase I metabolites in S9. The selective inhibitors and concentrations of quinone oxidoreductase 1 (NQO1) and aldehyde oxidase (AOX) used were as follows: dicumarol (50 $\mu\text{mol/L}$), and chlorpromazine (100 $\mu\text{mol/L}$)^[21, 23]. Cryptotanshinone (2 $\mu\text{mol/L}$) was incubated with S9 (0.2 mg/mL) and NADPH for 30 min in the presence of chemical inhibitors under the above-described conditions. Control incubations without the chemical inhibitors were also performed. The formation of m/z 473 metabolites was quantified by LC-MS/MS.

Sample preparation

The samples were vortexed and centrifuged at 12000 r/min for 10 min. The supernatant was collected and subjected to analysis by HPLC-MS/MS.

Sample analysis conditions

A hybrid quadrupole linear ion trap mass spectrometer (QTRAP) was used to quantitatively analyze cryptotanshinone and its metabolites, and a quadrupole-time of flight (QTOF) mass spectrometer was used to accurately determine the masses of the metabolites of cryptotanshinone. Simultaneous determination of the metabolic stability and metabolite identity was performed using QTRAP mass spectrometry.

Cryptotanshinone and its metabolites were investigated in various experiments by LC-MS/MS. An Agilent 1260 system (Agilent Technologies, Santa Clara, CA, USA) that included a vacuum degasser and quaternary pump was used for solvent and sample delivery. An Agilent Eclipse XDB-C18 instru-

ment (4.6 mm \times 150 mm, 3.5 μm , Agilent Technologies, USA) was used to separate each analyte for LC-MS/MS. The mobile phase consisted of solution A (0.1% formic acid, *v/v*) and solution B (ethanol) with a gradient of solution B (35%, 0–1.5 min; 35%–90%, 1.5–6.0 min; 90%, 6.0–16.4 min; and 35%, 16.5–20 min; *v/v*) at a flow rate of 0.3 mL/min. An API 4000 QTRAP mass spectrometer fitted with a Turbo IonSpray electrospray ionization instrument (AB Sciex, Framingham, MA) was used for mass spectrometry and detection. Analyst ver.1.6.2 and Lightsight ver.2.3 software (AB Sciex) were used for data acquisition and processing. The mass spectrometric data of the metabolites were confirmed using information-dependent acquisition experiments under the positive ion mode. Then, multiple reaction monitoring (MRM) analysis of the metabolites of cryptotanshinone was undertaken, revealing mass transitions of m/z 297.3 \rightarrow 251.2 for cryptotanshinone; m/z 295.3 \rightarrow 251.3 for the dehydrogenated forms; m/z 313.3 \rightarrow 249.3 for the hydroxylated forms; m/z 473.3 \rightarrow 297.3 for the glucuronidation forms; m/z 489.3 \rightarrow 313.3 for the glucuronidation forms; and m/z 285.2 \rightarrow 193.1 for the internal standard (IS). The declustering potential was set at 104 eV, the collision energy was set at 33 eV, and the collision cell exit potential was set at 12 eV for analysis of all of the analytes. The other parameters were set as follows: curtain gas, 15 psi; ion spray voltage, 5000 eV; temperature, 500°C; Gas₁, 50 psi; Gas₂, 50 psi; and collision-activated dissociation gas, 5 psi.

Authentic standards of the metabolites (except M1-3) were not available, so semi-quantitative analysis was conducted using the peak area. Low, medium and high contents of metabolites were produced in the microsomal incubation system by three different concentrations of cryptotanshinone. The intra-assay and inter-assay coefficients of the variation of determination of cryptotanshinone and its metabolites were <14.6%. No ionization suppression against cryptotanshinone and its metabolites was observed. For metabolite identification, accurate mass determination of the parent compound and its metabolites was performed on an Agilent 6530 QTOF mass spectrometer (Agilent, Santa Clara, CA, USA). The instrument was equipped with Dual Agilent Jet Stream Electrospray Ionization (Dual AJS ESI) and operated in the positive ion mode with the following parameters: sheath and drying gas (N₂, flow rate 10 L/min), drying gas temperature (300°C), nebulizing gas pressure (45 psi), sheath gas temperature (350°C), mass scan range (100–1000), skimmer (65 eV), capillary voltage (3500 eV), fragment (150 eV), and collision energy (15 eV). Mass Hunter Workstation, a software package for the 6530 series QTOF, was used to control all of the acquisition parameters and process the obtained data. The LC system and conditions were the same as above.

Data analysis

The data points represent the mean of duplicate estimates. $CL_{\text{int}(in vitro)}$ was determined via substrate depletion: $CL_{\text{int}(in vitro)} = k \times V/P$, $k = -\ln([S_1]/[S_0]) / (t_1 - t_0)$, where V represents the volume of the incubation system and P represents the microsomal protein of the incubation system. The value t_1 represents the

time (min) of incubation, and t_0 represents the initial incubation time. S_1 represents the substrate concentration at the end of t_1 , and S_0 represents the initial substrate concentration. $CL_{int(liver)} = CL_{int(in vitro)} \times MPPGL \times \text{liver weight}$, assuming an average value of microsomal protein per gram of liver (MPPGL) of 32 mg/g and a liver weight of 1480 g/70 kg.

The relative contributions of each CYP to cryptotanshinone in human liver microsomes were determined using the fraction metabolized (fm). The fm value was determined from their incubation in the presence and absence of specific inhibitors in HLMs. The initial rate of disappearance (k) of cryptotanshinone in the presence ($k_{with\ inh}$) and absence of ($k_{no\ inh}$) of inhibitors was determined as described above. fm was calculated as described by Yang et al^[24].

$$\% \text{ inhibition} = 100 \times \frac{k_{no\ inh} - k_{with\ inh}}{k_{no\ inh}}$$

$$fm = \frac{\% \text{ inhibition}}{\text{Sum of total \% inhibition across CYPs}}$$

Data are expressed as the mean \pm SD. Multiple comparisons were performed with one-way ANOVAs. $P < 0.05$ was considered statistically significant.

Results

Fifty-two proposed metabolites were detected by LC-MS/MS, specifically triple quadrupole linear ion trap mass spectrometry, and LightsightTM software using predictive MRM-IDA-EPI in HLMs in the presence of NADPH+UDPGA. There were 52 metabolites, including dehydrogenation, loss of water, oxidation, di-oxidation, demethylation, di-demethylation, and glucuronidation forms. Cryptotanshinone and its major phase I and phase II metabolites in human liver microsomes are presented in Table 1. The product ions and retention times of cryptotanshinone as well as these main metabolites in HLMs using QTRAP and QTOF are also summarized in Table 1.

Identification of cryptotanshinone phase I metabolites

M1-1, M1-2 and M1-3 were eluted at 10.47, 11.20 and 12.61 min, respectively. Those metabolites had an ion $[M+H]^+$ at m/z of 295, which suggested that these metabolites might be the dehydrogenated metabolites of cryptotanshinone. The MS² spectra of protonated M1-1, M1-2 and M1-3 revealed that the main fragment ions were 2 Da less than those of cryptotanshinone (Table 1). The MS² spectra of M1-3 were the same as those of tanshinone IIA. Therefore, M1-3 was confirmed as tanshinone IIA. According to the literature, M1-1 and M1-2 were identified as 1,2-dehydrocryptotanshinone or 2,3-dehydrocryptotanshinone^[25].

M2-1, M2-2 and M2-3 were eluted at 9.12, 9.31 and 10.47 min, respectively. These metabolites had an ion $[M+H]^+$ at m/z of 313, which is 16 Da heavier than that of cryptotanshinone. An obvious $[M+H-18]^+$ ion at m/z of 295, formed by the loss of H₂O, was observed in the MS/MS spectrum. The major product ions are shown in Table 1. This information indicated that M2-1, M2-2 and M2-3 were metabolites of cryptotanshinone with one hydroxyl group.

M3-1, M3-2 and M3-3 were eluted at 11.12, 11.32 and 11.68 min, respectively. These metabolites had a protonated molecule $[M+H]^+$ at m/z of 473. The MS/MS spectrum of these metabolites showed an intense ion at m/z of 295 corresponding to the neutral loss of 176 Da; incubation of HLM with β -glucuronidase resulted in the disappearance of these peaks from the chromatogram. This result indicated that M3-1, M3-2 and M3-3 were the glucuronide conjugate. The fragment ions of M3 at m/z of 295, 277 and 249 were similar to those of cryptotanshinone and were 2 Da heavier than those of dehydrocryptotanshinone. The product ion at m/z of 295 was proposed to be the hydrogenated product of dehydrocryptotanshinone, which is a semiquinone with a hydroxyl group at the C-11 or C-12 position. M3 was proposed to be the glucuronide conjugate of hydrogenated dehydrocryptotanshinone.

M4-1 and M4-2 were eluted at 8.21 and 8.58 min, respectively. Both of these metabolites had an $[M+H]^+$ ion at m/z of

Table 1. Mass spectrometric data of cryptotanshinone and its main metabolites.

ID	Rt	Biotransformation	Observed mass	MS2	Q1/Q3	Peak area
Parent	11.50		297.1487	297,282,279,268,254,251,249,221,209,193	297.3/251.0	9.12 $\times 10^6$
M1-1	10.47	Dehydrogenation	295.1326	295,280,277,265,262,251,249,247,234,226,220,216,212	295.3/251.0	2.44 $\times 10^4$
M1-2	11.20	Dehydrogenation	295.1333	295,280,277,262,251,249,247,234,220,206,195	295.3/251.0	7.77 $\times 10^5$
M1-3	12.61	Dehydrogenation	295.1306	295,280,277,265,251,249,234,221,206,191,179	295.3/251.0	8.17 $\times 10^4$
M2-1	9.12	Hydroxylation	313.1437	313,295,282,270,267,262,249,234,229,224,221,209,206	313.3/251.0	1.44 $\times 10^5$
M2-2	9.31	Hydroxylation	313.1423	313,295,277,267,262,249,235,225,221,206,195,185	313.3/251.0	8.47 $\times 10^5$
M2-3	10.47	Hydroxylation	313.1423	313,295,277,262,249,225,206,195,185,167,142	313.3/251.0	7.30 $\times 10^4$
M3-1	11.12	Glucuronidation	473.1801	473,297,279,251,237,223,178	473.3/297.3	4.31 $\times 10^4$
M3-2	11.32	Glucuronidation	473.1801	473,309,297,279,254, 251,223	473.3/297.3	2.58 $\times 10^4$
M3-3	11.68	Glucuronidation	473.1801	473,309,297,279,251,236,223	473.3/297.3	3.03 $\times 10^4$
M4-1	8.21	Hydroxylation plus glucuronidation	489.1761	489,313,297,280,249,128	489.3/313.3	3.82 $\times 10^4$
M4-2	8.56	Hydroxylation plus glucuronidation	489.1754	489,313,295,277,267,252,249,225	489.3/313.3	3.95 $\times 10^4$

489. The MS/MS spectrum of M4 showed an intense ion at m/z of 313 corresponding to the neutral loss of 176 Da. Incubation of HLM with β -glucuronidase resulted in the disappearance of M4-1 and M4-2. This result indicated that M4-1 and M4-2 were the glucuronide conjugate of the hydroxyl metabolites of cryptotanshinone. The product ion spectra of M4-1 and M4-2 were similar, which indicated that these metabolites might be

isomers.

Metabolic stability and the metabolic reactions of cryptotanshinone in HLMs were evaluated.

Based on the peak areas of the metabolites observed via LC-MS/MS using information-dependent acquisition experiments under the positive ion mode, eleven metabolites of cryptotanshinone were selected for multiple reaction monitor-

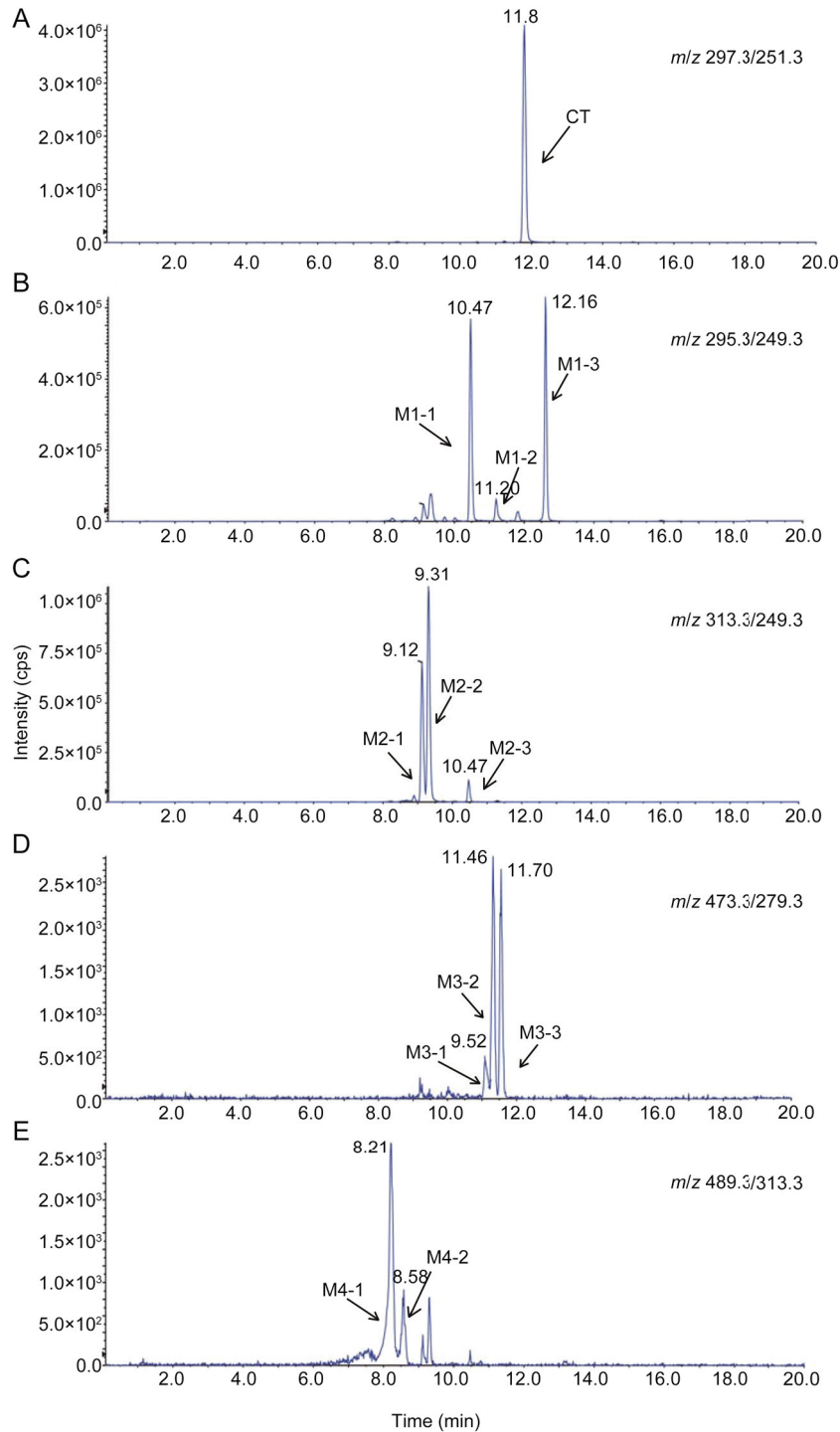


Figure 1. MRM chromatograms of CT and its metabolites in HLMs. These chromatograms show the formation of (A) unchanged, (B) dehydrogenated, (C) hydroxylated, (D) glucuronidation forms, and (E) glucuronidation forms of CT in HLMs.

ing. MRM analysis of the metabolites of cryptotanshinone with mass transitions (m/z) of 297.3→251.3, 295.3→249.3, and 313.3→249.3 was the unchanged, dehydrogenated, and hydroxylated forms, respectively. Glucuronidation products were represented by mass transitions (m/z) of 473.3→279.3 and 489.3→313.3 (Figure 1).

To determine the NADPH- and NADPH+UDPGA-dependent metabolic stability of cryptotanshinone, the disappearance of the parent compound was measured at six time points between 0 and 60 min in HLM in the presence of NADPH or NADPH+UDPGA. More than 50% of cryptotanshinone was eliminated within 20 min in the presence of NADPH+UDPGA, but comparable depletion occurred over more than 30 min in the presence of NADPH. The CL_{int} (*in vitro*) values of cryptotanshinone were 1.61 and 2.38 mL·h⁻¹·mg⁻¹ in the presence of NADPH and NADPH+UDPGA, respectively. Subsequently, the CL_{int} (*liver*) values of cryptotanshinone were 76.4 and 112.9 L/h in the presence of NADPH and NADPH+UDPGA, respectively. HLMs can generate some phase I and phase II metabolites of cryptotanshinone that are extensively metabolized in the liver by UGTs after CYPs.

The eleven main metabolites of cryptotanshinone were selected to plot the peak area-time curves over a 60-min incubation in NADPH or NADPH+UDPGA (Figure 2). The formation of M1-1, M1-2, M1-3, M2-1, M2-2, and M2-3 increased for over 1 h in HLMs with NADPH. The formation of the six phase I metabolites decreased after 10 to 30 min, whereas the formation of five phase II metabolites (M3-1, M3-2, M3-3 and M4-1, M4-2) increased for over 1 h in HLMs with NADPH and UDPGA, which indicated that phase I metabolites might be transformed into phase II metabolites by HLMs with NADPH and UDPGA.

Identification of CYPs responsible for the metabolism of cryptotanshinone in human liver microsomes

Selective inhibitors of the seven major CYPs were used to identify the CYP isozymes responsible for cryptotanshinone metabolism in HLMs. As shown in Figure 3 and Table 2, cryptotanshinone was metabolized by CYPs in HLMs with NADPH in the control group. Inhibition (%) of cryptotanshinone metabolism in HLMs with NADPH and the inhibitors of CYP1A2, CYP2A6, CYP2C19 and CYP3A4 were 35.8%, 57.6%, 58.0% and 50.0%, respectively ($P<0.05$). These results suggested that CYP1A2, CYP2A6, CYP2C19 or CYP3A4 may be responsible for cryptotanshinone metabolism in HLMs. Furthermore, the f_m values of the total cryptotanshinone metabolism by CYP2C19, CYP2A6, CYP3A4, and CYP1A2 were 25.9%, 25.7%, 22.3%, and 16.0%, respectively, as shown in Table 2. By contrast, only marginal inhibition (<10%) was observed with either CYP2C8 or CYP2C9. Therefore, CYP2C19, CYP2A6, CYP3A4 or CYP1A2 might be the principal P450 isozymes involved in the formation of phase I metabolites.

Assay with recombinant human CYPs

To further confirm the CYP isoforms involved in the metabolism of cryptotanshinone, the catalytic activities of 7 individual

Table 2. The contribution and f_m of CYPs to cryptotanshinone metabolism in HLMs.

CYP enzymes	% Inhibition	f_m (%)
1A2	35.8	16.0
2A6	57.6	25.7
2C8	14.1	6.3
2C9	1.5	0.7
2C19	58.0	25.9
2D6	7.0	3.1
3A4	50.0	22.3

recombinant human CYP isoforms (rCYP) were evaluated. As shown in Figure 4, rCYP1A2, rCYP2A6, rCYP2C19 or rCYP3A4 may play a major role in cryptotanshinone metabolism.

As shown in Figure 4, rCYP2C19 had the largest role in the formation of M1-1, M1-3 and M2-3, although rCYP1A2 was also involved in the formation of M1-1 and M2-3. The rCYP2A6 isoform showed the highest metabolic activity in reactions forming M2-2, although the rCYP3A4 isoform also showed potent metabolic activity in reactions forming M2-1 and M2-2. These results further confirmed the roles of CYP2C19, CYP2A6 and CYP3A4 in cryptotanshinone phase I metabolism. Moreover, rCYP2C8 and rCYP2D6 participated in cryptotanshinone phase I metabolism to some extent.

Identification of UGT isoforms involved in the glucuronidation of cryptotanshinone

Glucuronidation of cryptotanshinone by 12 commercially available isoforms of rUGT was measured with 10 μmol/L cryptotanshinone. The reduced catechol intermediate was not detected by LC-MS/MS after the supernatant was dried after cryptotanshinone incubation with NADPH. Thus, human liver cytosol was added as the NQO1 donor to produce reduced cryptotanshinone or its metabolites.

As shown in Figure 4C, UGT1A9 was the dominant enzyme involved in the formation of M3-2 and M3-3 from reduced dehydrocryptotanshinone. As shown in Figure 4D, glucuronidation of hydroxylated metabolites was catalyzed primarily by UGT2B7 with minor contributions from UGT2B4.

Given the lack of specific inhibitors for UGTs, diclofenac sodium has been shown to be a selective inhibitor of UGT1A9, 2B4, and 2B7^[22, 24]. Thus, the potential inhibitory effect of diclofenac sodium was investigated in cryptotanshinone glucuronidation. Inhibition (%) of cryptotanshinone metabolism was 50% in HLMs with NADPH and UDPGA in the presence of diclofenac sodium (300 μmol/L). This result suggested that UGT1A9, UGT2B4 and UGT2B7 were also important contributors to cryptotanshinone metabolism.

Identification of the enzymes that catalyze the reduction of M1 in S9

Selective chemical inhibitors were used to investigate the

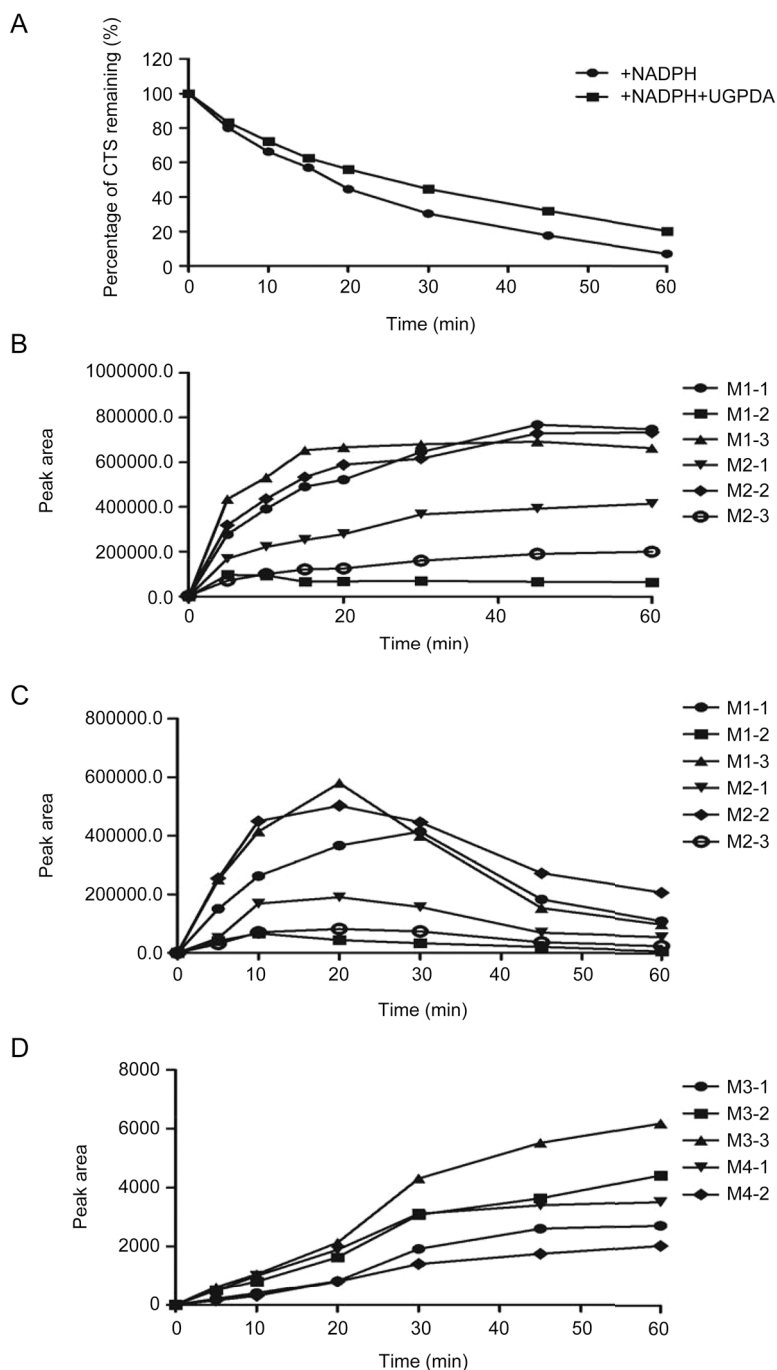


Figure 2. Time course of degradation of cryptotanshinone during a 60-min incubation in HLMs (A) and the generation of its main metabolites, including M1-1, M1-2, M1-3, M2-1, M2-2, and M2-3 in NADPH (B), M1-1, M1-2, M1-3, M2-1, M2-2, and M2-3 (C), M3-1, M3-2, M3-3, M4-1 and M4-2 (D) in NADPH+UDPGA.

enzymes responsible for the reduction of cryptotanshinone and its phase I metabolites in S9. Dicumarol and chlorpromazine were used as selective inhibitors of NQO1 and AOX. We found that the formation of *m/z* of 473 metabolites was effectively inhibited (up to 94%) by dicumarol (a NQO1 inhibitor) in the presence of NADPH in S9. By contrast, no inhibition was observed with chlorpromazine (an AOX inhibitor). Since NQO1 is mainly distributed in the cytosol, this study used

human liver cytosol as the NQO1 donor to produce reduced cryptotanshinone, which was then subjected to glucuronidation screening with a panel of 12 commercially available isoforms of rUGT.

On the basis of the present work, the 11 main metabolites of cryptotanshinone were detected and characterized in human liver microsomes. A possible metabolic pathway of cryptotanshinone in human liver microsomes was proposed, as shown

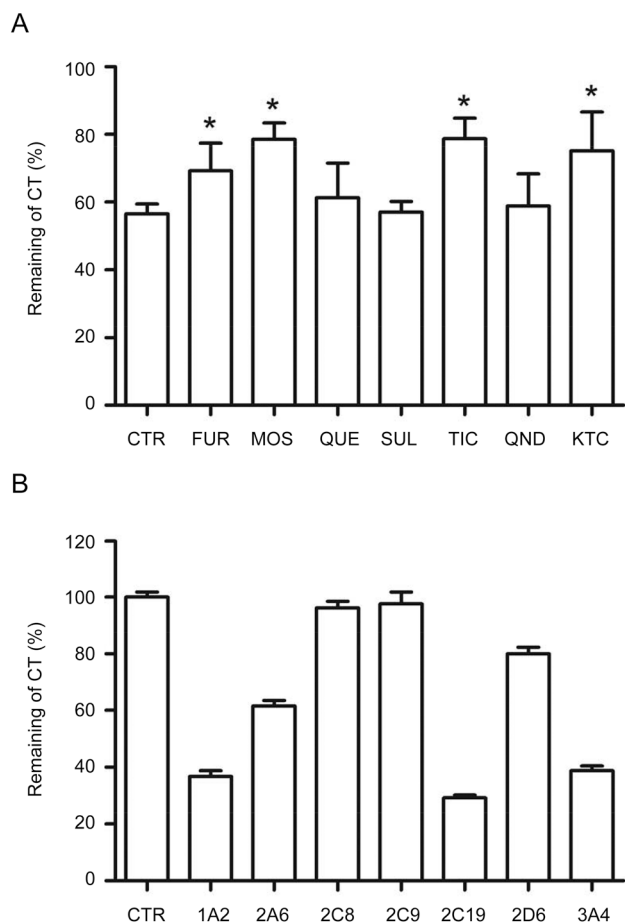


Figure 3. (A) Effects of various chemical inhibitors of CYP enzymes on CTS metabolism in HLM (KTC: ketoconazole, QND: quinidine, FUR: Furafylline, MOS: methoxsalen, QUE: quercetin, SUL: sulfaphenazole, TIC: ticlopidine). (B) The metabolism of cryptotanshinone by CYP recombinant enzymes. * $P < 0.05$ vs control group.

in Figure 5. The six phase I metabolites were formed from two main metabolic routes: hydroxylation and dehydrogenation metabolism. Glucuronide conjugates of semiquinones were proposed as the five phase II metabolites, and semiquinones or hydroxylations were the hydrogenated products of dehydrocryptotanshinone M3-1, M3-2, and M3-3.

These results suggested that cryptotanshinone underwent hydroxylation metabolism or dehydrogenation, further quinone reduction metabolism, and subsequent glucuronidation.

Discussion

In this study, the metabolic characteristics of cryptotanshinone were first investigated in HLMs as well as recombinant human CYP and UGT enzymes. We identified forty-seven phase I metabolites, including loss of water, oxidation, di-oxidation, demethylation, di-demethylation furan ring cleavage metabolites, and five glucuronide conjugation phase II metabolites. We found that cryptotanshinone underwent extensive phase I and phase II metabolism in HLMs. Based on the metabolite profile, hydroxylation and dehydrogenation metabolism were

the two main metabolic routes, which involved six phase I metabolites (M1-1, M1-2, and M1-3; and M2-1, M2-2 and M2-3). M1-1, M1-2, and M1-3 were dehydrogenated metabolites, whereas M2-1, M2-2, and M2-3 were hydroxylated metabolites. These findings were similar to a previous study that incubated cryptotanshinone and NADPH in rat and pig liver microsomes^[11,12]. After adding UDPGA to the incubation system, another five main phase II metabolites (M3-1, M3-2, M3-3, M4-1, and M4-2) were identified as glucuronide conjugates. When cryptotanshinone was incubated in HLMs with UDPGA, no glucuronidation of cryptotanshinone was found, so cryptotanshinone cannot directly conjugate with glucuronic acid without a hydroxyl group, as opposed to tanshinone IIA^[17].

Characterization of drug metabolic properties, including metabolic stability, can play a critical role in the safe use of drugs in clinical medicine. When lacking authentic metabolite standards, metabolic stability is usually quantified by monitoring the disappearance of the parent compound over time in an *in vitro* system to determine the intrinsic clearance (CL_{int}). In HLMs, the CL_{int} (*in vitro*) of cryptotanshinone was 1.61 and 2.38 $mL \cdot h^{-1} \cdot mg^{-1}$ in the presence of NADPH and NADPH+UDPGA, respectively. Using the IVIVE method, the CL_{int} in the human liver was 76.4 or 112.9 L/h, which suggested that cryptotanshinone was metabolized extensively in the liver^[26]. In this study, metabolism of cryptotanshinone in the presence of NADPH and UDPGA better reflected cryptotanshinone metabolism *in vivo*. The CYP3A4 enzyme, which is expressed abundantly in the gastrointestinal tract and liver, was the main enzyme responsible for the formation of phase I hydroxylated metabolites from cryptotanshinone. Therefore, cryptotanshinone probably suffered intensive metabolism in the liver and intestinal tract mediated by CYPs and UGTs, which resulted in the low bioavailability of cryptotanshinone. The involvement of CYP isoforms in cryptotanshinone metabolism was studied by chemical inhibition in HLMs and using recombinant human CYPs. CYP2C19, CYP2A6, CYP3A4, and CYP1A2 inhibited cryptotanshinone metabolism by 58.0%, 57.6%, 50.0%, and 35.8%, respectively. The *fm* values of CYP2C19, CYP2A6, CYP3A4, and CYP1A2 in HLMs were 25.9%, 25.7%, 22.3%, and 16.0%, respectively, indicating that these enzymes were the major contributors to cryptotanshinone metabolism. CYP2C19, CYP1A2 and CYP3A4 were responsible for dehydrogenation, whereas CYP2A6, CYP3A4, and CYP2C19 were responsible for hydroxylation. Liu *et al*^[27] found that CYP2A6 was the specific isozyme responsible for hydroxylation of tanshinone IIA in human liver microsomes. In the present study, we found that the hydroxyl metabolite (M2-3) was also formed by CYP2A6, although a topic for future research is whether the hydroxylation position is the same. At first, the dehydrogenation metabolites of cryptotanshinone were reported as being mainly catalyzed by CYP2C19 and CYP1A2. Furthermore, the dehydroxylated metabolites of cryptotanshinone were mainly catalyzed by CYP2A6.

The phase II metabolite observed for the $[M+H]^+$ ion at 473 might be the glucuronide conjugate of the semiquinone of

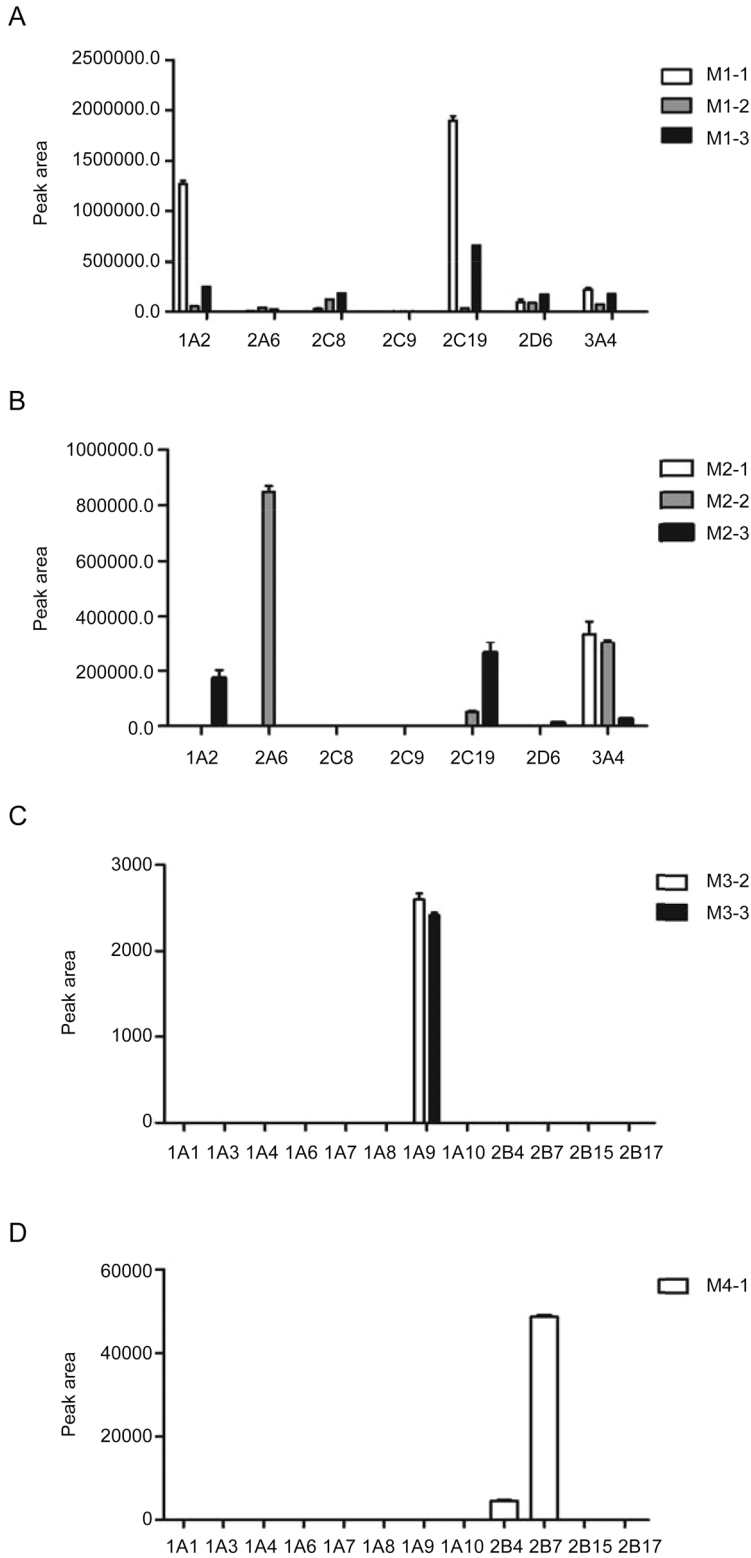


Figure 4. (A) Formation of the dehydrogenation metabolites (M1-1, M1-2 and M1-3) from cryptotanshinone using human cDNA-expressed CYP isoforms. Cryptotanshinone at 10 $\mu\text{mol/L}$ was incubated with each recombinant CYP isoform (CYP1A2, 2A6, 2C8, 2C9, 2C19, 2D6 and 3A4). (B) Formation of hydroxylation metabolites from cryptotanshinone using human cDNA-expressed CYP isoforms. Cryptotanshinone at 10 $\mu\text{mol/L}$ was incubated with each recombinant CYP isoform (CYP1A2, 2A6, 2C8, 2C9, 2C19, 2D6 and 3A4). (C) Formation of cryptotanshinone glucuronide from cryptotanshinone using human cDNA-expressed UGT isoforms. Cryptotanshinone at 10 $\mu\text{mol/L}$ was incubated with each recombinant UGT isoform (UGT1A1, 1A3, 1A4, 1A6, 1A7, 1A8, 1A9, 1A10, 2B4, 2B7, 2B15 and 2B17). Each bar represents the mean \pm standard deviation (SD) of triplicate determinations. (D) Formation of cryptotanshinone glucuronide (m/z of 489) from cryptotanshinone using human cDNA-expressed UGT isoforms. Cryptotanshinone at 10 $\mu\text{mol/L}$ was incubated with each recombinant UGT isoform (UGT1A1, 1A3, 1A4, 1A6, 1A7, 1A8, 1A9, 1A10, 2B4, 2B7, 2B15 and 2B17). Each bar represents the mean \pm standard deviation (SD) of triplicate determinations.

dehydrocryptotanshinone. The product ion at m/z of 297 was proposed to be the hydrogenized product of dehydrocryptotanshinone, which is a semiquinone with a hydroxyl group at the C-11 or C-12 position. In this study, the formation of m/z of 473 metabolites was effectively inhibited by NQO1

(dicumarol), whereas no inhibition was observed with AOX (chlorpromazine) in S9. Wang *et al*^[22] reported that NQO1 catalyzed a quinone reduction, producing a highly unstable catechol intermediate followed by an immediate glucuronidation and that this pathway was the predominant metabolic

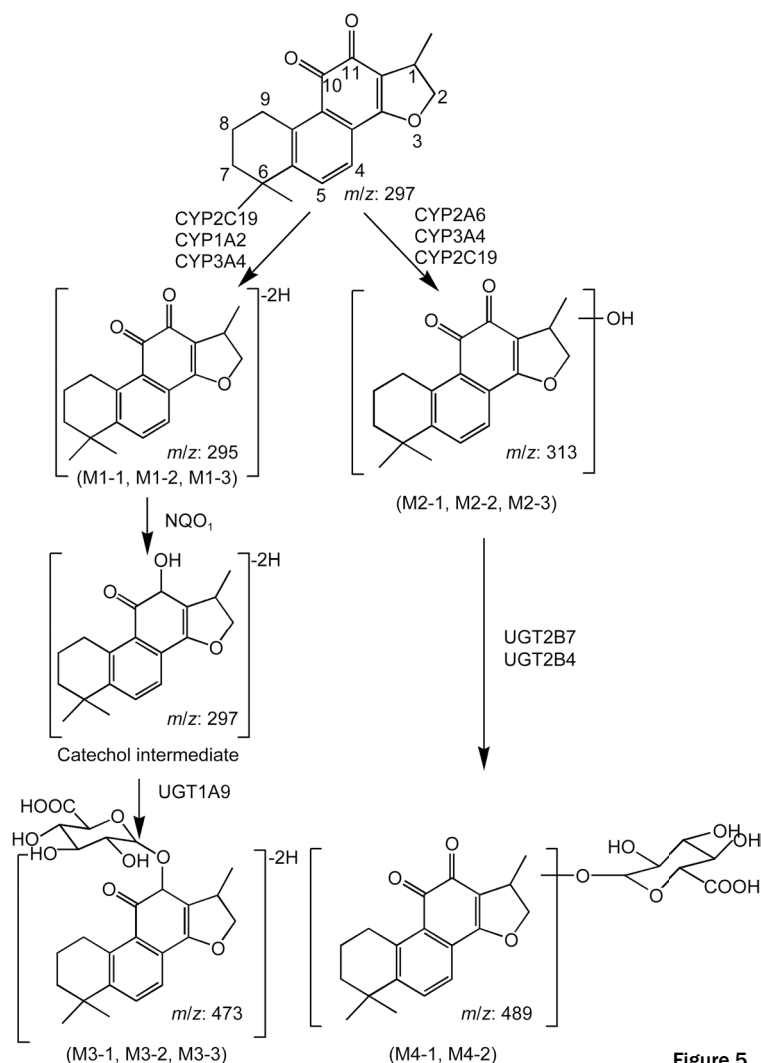


Figure 5. The proposed metabolic pathway of cryptotanshinone in HLMs.

pathway of tanshinone IIA. The results indicated that NQO1 mediated both quinone reduction of dehydrocryptotanshinone and the subsequent glucuronidation catalyzed by UGT1A9. The metabolite at m/z of 475 was found by Q1 scanning with QTOF of the incubation samples, but the peak area was less than that of the metabolite at m/z of 473 (data not shown).

Although NQO1 is mainly distributed in the cytosol^[20], there is a small amount in human liver microsomes. In the present study, the peak area of the metabolite at m/z of 473 was higher than that of the metabolite at m/z of 489 in HLMs. Because there was a larger amount of NQO1 enzyme in the cytosol than in HLMs, there is much more of the metabolite at m/z of 473 in the human body. This result suggested that NQO1-mediated quinone reduction of dehydrocryptotanshinone and the subsequent glucuronidation catalyzed by UGT1A9 was the major phase II metabolic pathway for cryptotanshinone.

Glucuronidation of hydroxylated metabolites was primarily catalyzed by UGT2B7 with minor contributions from UGT2B4. Lacking UGT2B4 and UGT2B7 expression in the intestinal tract, the metabolite at m/z of 489 was possibly metabolized in the liver by glucuronidation of UGT2B7 and UGT2B4

followed by hydroxylation of CYP.

The main drug metabolizing enzymes for cryptotanshinone were CYP2C19, CYP1A2, CYP2A6, CYP3A4, UGT1A9 and UGT2B7. Genetic variations of CYP2C19, CYP2A6, CYP1A2, CYP3A4, UGT1A9, UGT2B7 and CYP3A4 have been reported in humans, and the polymorphic nature of CYPs and UGTs could affect individual drug exposure to a great extent^[28-33]. Therefore, potential individual differences in pharmacological responses to cryptotanshinone might occur due to differential metabolic capacity.

Cryptotanshinone was metabolized by CYP2C19, CYP1A2, CYP2A6, CYP3A4, UGT1A9 and UGT2B7. We found that cryptotanshinone induced CYP3A4 and P-gp activity in human liver hepatocytes^[8]. Yu reported that cryptotanshinone activated the pregnane X receptor (PXR) and consequently induced expression of CYP2C19, UGT1A9 and UGT2B7, which are the target genes of PXR^[34]. Zhang reported that cryptotanshinone also induced CYP1A2^[35]. Long-term administration of cryptotanshinone induced CYP2C19, CYP1A2, CYP3A4, UGT1A9 and UGT2B7 to enhance cryptotanshinone metabolism in the liver. The exposure of the human body to crypto-

tanshinone would be reduced, possibly leading to tolerance of cryptotanshinone.

In conclusion, we characterized the metabolism of cryptotanshinone by the CYP and UGT enzymes using liver microsomes and recombinant human drug metabolic enzymes. NADPH-supplemented HLM generated six main dehydrogenation and hydroxylation metabolites from cryptotanshinone, and UDPGA-supplemented liver microsomes generated five main phase II glucuronidation metabolites. This study shows for the first time that CYP2A6, CYP3A4 and CYP2C19 are the major contributors to the transformation of cryptotanshinone hydroxylation metabolites and that CYP2C19, CYP1A2 and CYP3A4 are the major contributors to the transformation of its hydrogenation metabolites in human liver microsomes. This study also shows that the metabolite at *m/z* of 473 was mediated by UGT1A9 and the metabolite at *m/z* of 489 was mediated by UGT2B7 and UGT2B4. Elucidation of the CT metabolic pathways and metabolic enzymes is useful not only to understand CT metabolism but also to predict likely drug interactions of Western medicines that are used concomitantly in clinical treatment.

Acknowledgements

This work was supported by the National Natural Science Foundation of China (No 81173118) and Shanghai Key Lab of Traditional Clinical Medicine (Grant C14dZ2273200).

Author contribution

Fu-rong QIU and Jian JIANG participated in research design. Jin ZENG, Yu-juan FAN, Yue LI, and Lin-lin ZHANG performed experiments. Jin ZENG, Yu-juan FAN, Hui-zong SU, Lin-lin ZHANG and Fu-rong QIU performed data analysis. Fu-rong QIU and Bo TAN contributed to the writing of the manuscript.

References

- Cheng TO. Cardiovascular effects of danshen. *Int J Cardiol* 2007; 121: 9–22.
- Lee DS, Lee SH, Noh JG, Hong SD. Antibacterial activities of cryptotanshinone and dihydrotanshinone I from a medicinal herb, *Salvia miltiorrhiza* Bunge. *Biosci Biotechnol Biochem* 1999; 63: 2236–9.
- Jin DZ, Yin LL, Ji XQ, Zhu XZ. Cryptotanshinone inhibits cyclooxygenase-2 enzyme activity but not its expression. *Eur J Pharmacol* 2006; 549: 166–72.
- Kang BY, Chung SW, Kim SH, Ryu SY, Kim TS. Inhibition of interleukin-12 and interferon-gamma production in immune cells by tanshinones from *Salvia miltiorrhiza*. *Immunopharmacology* 2000; 49: 355–61.
- Chen W, Liu L, Luo Y, Odaka Y, Awate S, Zhou H, et al. Cryptotanshinone activates p38/JNK and inhibits Erk1/2 leading to caspase-independent cell death in tumor cells. *Cancer Prev Res* 2012; 5: 778–87.
- Xue M, Cui Y, Wang HQ, Luo YJ, Zhang B, Zhou ZT. Pharmacokinetics of cryptotanshinone and its metabolite in pigs. *Acta Pharm Sin* 1999; 34: 81–4.
- Xie MZ, Shen ZF. Absorption, distribution, excretion and metabolism of cryptotanshinone. *Acta Pharm Sin* 1983; 18: 90–6.
- Qiu F, Jiang J, Ma Y, Wang G, Gao C, Zhang X, et al. Opposite effects of single-dose and multidose administration of the ethanol extract of Danshen on CYP3A in healthy volunteers. *Evid Based Complement Alternat Med* 2013; 730734: 1–8.
- Zhang J, Huang M, Guan S, Bi HC, Pan Y, Duan W. A mechanistic study of the intestinal absorption of cryptotanshinone, the major active constituent of *Salvia miltiorrhiza*. *J Pharmacol Exp Ther* 2006; 317: 1285–94.
- Dai H, Li X, Bai L, Li Y, Xue M. Coexisted components of *Salvia miltiorrhiza* enhance intestinal absorption of cryptotanshinone via inhibition of the intestinal P-gp. *Phytomedicine* 2012; 19: 1256–62.
- Gao Y, Shao J, Jiang Z, Chen J, Gu S, Yu S. Drug enterohepatic circulation and disposition: constituents of systems pharmacokinetics. *Drug Discov Today* 2014; 19: 326–40.
- Song M, Hang TJ, Zhang ZX, Du R, Chen J. Determination of cryptotanshinone and its metabolite in rat plasma by liquid chromatography-tandem mass spectrometry. *J Chromatogr B Analyt Technol Biomed Life Sci* 2005; 827: 205–9.
- Dai H, Wang M, Li X, Wang L, Li Y, Xue M. Structural elucidation of *in vitro* and *in vivo* metabolites of cryptotanshinone by HPLC-DAD-ESI-MS(n). *J Pharm Biomed Anal* 2008; 48: 885–96.
- Liu J, Wu J, Wang X, Cao Z. Study of the phase I and phase II metabolism of a mixture containing multiple tanshinones using liquid chromatography/tandem mass spectrometry. *Rapid Commun Mass Spectrom* 2007; 21: 2992–8.
- Zanger UM, Schwab M. Cytochrome P450 enzymes in drug metabolism: regulation of gene expression, enzyme activities, and impact of genetic variation. *Pharmacol Ther* 2013; 138: 103–41.
- Kiang TK, Ensom MH, Chang TK. UDP-glucuronosyltransferases and clinical drug-drug interactions. *Pharmacol Ther* 2005; 106: 97–132.
- Emoto C, Murayama N, Rostami-Hodjegan A, Yamazaki H. Methodologies for investigating drug metabolism at the early drug discovery stage: prediction of hepatic drug clearance and P450 contribution. *Curr Drug Metab* 2010; 11: 678–85.
- Fan G, Jiang X, Wu X, Fordjour PA, Miao L, Zhang H, et al. Anti-inflammatory activity of tanshinone IIA in LPS-stimulated RAW264.7 macrophages via miRNAs and TLR4-NF-κB pathway. *Inflammation* 2016; 39: 375–84.
- Xie J, Liu J, Liu H, Liang S, Lin M, Gu Y, et al. The antitumor effect of tanshinone IIA on anti-proliferation and decreasing VEGF/VEGFR2 expression on the human non-small cell lung cancer A549 cell line. *Acta Pharm Sin B* 2015; 5: 554–63.
- Joo J, Kim YW, Wu Z, Shin JH, Lee B, Shon JC, et al. Screening of non-steroidal anti-inflammatory drugs for inhibitory effects on the activities of six UDP-glucuronosyltransferases (UGT1A1, 1A3, 1A4, 1A6, 1A9 and 2B7) using LC-MS/MS. *Biopharm Drug Dispos* 2015; 36: 258–64.
- Foti RS, Dalvie DK. Cytochrome P450 and non-cytochrome P450 oxidative metabolism: contributions to the pharmacokinetics, safety, and efficacy of xenobiotics. *Drug Metab Dispos* 2016; 44: 1229–45.
- Wang Q, Hao H, Zhu X, Yu G, Lai L, Liu Y, et al. Regioselective glucuronidation of tanshinone IIA after quinone reduction: identification of human UDP-glucuronosyltransferases, species difference and interaction potential. *Drug Metab Dispos* 2010; 38: 1132–40.
- Wu X, Zhang Q, Guo J, Jia Y, Zhang Z, Zhao M, et al. Metabolism of F18, a derivative of calanolide A, in human liver microsomes and cytosol. *Front Pharmacol* 2017; 8: 1–18.
- Yang X, Atkinson K, Di L. Novel cytochrome P450 reaction phenotyping for low clearance compounds using the hepatocyte relay method. *Drug Metab Dispos* 2016; 44: 460–5.
- Sun J, Yang M, Han J, Wang B, Ma X, Xu M, et al. Profiling the

- metabolic difference of seven tanshinones using high-performance liquid chromatography/multi-stage mass spectrometry with data-dependent acquisition. *Rapid Commun Mass Spectrom* 2007; 21: 2211–26.
- 26 Song YL, Jing WH, Yan R, Wang YT. Metabolic characterization of (\pm)-praeruptorin A *in vitro* and *in vivo* by high performance liquid chromatography coupled with hybrid triple quadrupole-linear ion trap mass spectrometry and time-of-flight mass spectrometry. *J Pharm Biomed Anal* 2014; 90: 98–110.
- 27 Liu HX, Hu Y, Liu Y, He YQ, Li W, Yang L. Hydroxylation of tanshinone IIA in human liver microsomes is specifically catalysed by cytochrome P4502A6. *Xenobiotica* 2009; 39: 382–90.
- 28 He P, Court MH, Greenblatt DJ, Von Moltke LL. Genotype-phenotype associations of cytochrome P450 3A4 and 3A5 polymorphism with midazolam clearance *in vivo*. *Clin Pharmacol Ther* 2005; 77: 373–87.
- 29 Özhan G1, Mutur M, Ercan G, Alpertunga B. Genetic variations in the xenobiotic-metabolizing enzymes CYP1A1, CYP1A2, CYP2C9, CYP2C19 and susceptibility to colorectal cancer among Turkish people. *Genet Test Mol Biomarkers* 2014; 18: 223–8.
- 30 Nurfadhlina M, Foong K, The LK, Tan SC, Mohd Zaki S, Ismail R. CYP2A6 polymorphisms in Malays, Chinese and Indians. *Xenobiotica* 2006; 36: 684–92.
- 31 Hu YR, Qiao HL, Kan QC. Pharmacokinetics of lansoprazole in Chinese healthy subjects in relation to CYP2C19 genotypes. *Acta Pharmacol Sin* 2004; 25: 986–90.
- 32 Court MH, Duan SX, von Moltke LL, Greenblatt DJ, Patten CJ, Miners JO. Interindividual variability in acetaminophen glucuronidation by human liver microsomes: identification of relevant acetaminophen UDP-glucuronosyltransferase isoforms. *J Pharmacol Exp Ther* 2001; 299: 998–1006.
- 33 Hwang MS, Lee SJ, Jeong HE, Lee S, Yoo MA, Shin JG. Genetic variations in UDP-glucuronosyltransferase 2B7 gene (UGT2B7) in a Korean population. *Drug Metab Pharmacokinet* 2010; 25: 398–402.
- 34 Yu C, Ye S, Sun H, Liu Y, Gao L, Shen C, et al. PXR-mediated transcriptional activation of CYP3A4 by cryptotanshinone and tanshinone IIA. *Chem Biol Interact* 2009; 177: 58–64.
- 35 Zhang R, Sun J, Ma L, Wu X, Pan G, Hao H. Induction of cytochromes P450 1A1 and 1A2 by tanshinones in human HepG2 hepatoma cell line. *Toxicol Appl Pharmacol* 2011; 252: 18–27.